J. Fluid Mech. (1989), *vol.* 198, *pp.* 429–451
Printed in Great Britain

Topology of a turbulent boundary layer with and without wall suction

By R. A. ANTONIA† AND L. FULACHIER‡

† Department of Mechanical Engineering, University of Newcastle, New South Wales, 2308, Australia

‡ Institut de Mécanique Statistique de la Turbulence, Université d'Aix-Marseille, 13003, Marseille, France

(Received 25 November 1987 and in revised form 28 June 1988)

Measurements of velocity and temperature fluctuations are made in a turbulent boundary layer with nominally zero pressure gradient for two different slightly heated wall conditions: impermeable and porous surfaces. The temperature fluctuations are measured at three points in the flow to permit the identification of two spatially coherent events: coolings and heatings. Conditional velocity vectors in the plane of mean shear are viewed in a reference frame which translates at a constant velocity. Conditioning is on coolings, heatings or a combination of these events. Sectional streamlines, derived from the velocity vector data, show a succession of critical points: saddles and unstable foci. Coolings are aligned with diverging separatrices through the saddles whereas heatings are identified with the foci. Coolings are associated with a large strain rate and also a large spanwise vorticity: this result seems consistent with the presence of hairpin vortices which extend to different distances from the wall. In contrast, the strain rate and spanwise vorticity are small at the foci. The stabilizing influence of suction is observed in the topology of the organized motion and in the contribution from this motion to the conventional stresses, temperature variance and heat fluxes.

1. Introduction

The structure of the boundary layer has been investigated using flow visualizations and hot-wire measurements, either separately or in combination, with different amounts of detail (see, for example, Willmarth 1975; Kline 1978). Most of the attention has focused on the outer region and the near-wall region. Less attention (e.g. Kline & Falco 1979) has been given to the interaction between these two regions. Brown & Thomas (1977) showed that the small-scale activity near the wall is correlated with the large-scale structure, more specifically with the upstream boundary of this structure. A similar correlation was found by Rajagopalan & Antonia (1979) in a fully developed turbulent duct flow. Chen & Blackwelder (1978) concluded that the temperature front, characterized by a spatially coherent rapid decrease in temperature with time and referred to here as a cooling, provided a plausible dynamic link between the bursting phenomenon and the large structure. Coolings were identified with the backs of bulges in the outer region of the boundary layer. Several of their characteristics have been obtained (Subramanian *et al.* 1982; Antonia *et al.* 1982). In a previous paper (Antonia *et al.* 1988, hereinafter referred to as I), the influence of suction on the structure of a turbulent boundary layer was assessed by comparing the characteristics of coolings over a porous wall with those

measured over an impervious wall. Also considered in I were the properties of heatings, characterized by a spatially coherent increase in temperature.

From conditionally averaged velocity components in the x- and y-directions Chen & Blackwelder constructed a composite picture of the two-dimensional velocity field associated with coolings. However, the local mean values of the two velocity components were subtracted from their picture (figure 18), so that evidence of large-scale organization is not discernible.

The major aim of the present paper is to determine the flow patterns associated with coolings and heatings and to use these patterns to discuss the physics of the organized motion. It was suggested in I that the coolings may be associated with vortex loops or hairpin vortices. An attempt is now made to quantify this association both from the topology of the organized motion and from contours of spanwise vorticity and strain rate which are conditioned on features of this motion. A second aim is to estimate the contribution that the organized motion makes to conventional stresses, temperature variance and heat fluxes. The effect of suction is examined with respect to the topology and the contribution of the organized motion to variances and fluxes.

2. Experimental details

A description of the experimental arrangement and conditions has been given in I. Here we give details of the measuring instruments and procedures relevant to this investigation. Also given is a justification of the experimental methodology which was adopted.

The turbulent boundary layer developed on the working section floor of the low-speed wind tunnel (0.56 m × 0.56 m). As shown in figure 1, wall suction could be applied at a distance of 3.05 m from the beginning of the working section. The measuring station was located at a distance of 640 mm from the start of the porous surface. Mean velocity profiles on the impervious and porous surfaces indicated that both surfaces were aerodynamically smooth. Measurements were made at a nominal free-stream velocity U_1 of 12.6 m/s for two values of V_w/U_1 (0 and -3×10^{-3}) or $A^+ = -V_w/U_\tau$ (0 and 0.055)†. Relevant experimental parameters are given in table 1.

The longitudinal and normal velocity fluctuations have been measured with an X-probe while temperature fluctuations were measured with cold wires. The arrangement of the wires is shown in figure 2. The hot wires were operated with DISA constant temperature circuits at a resistance ratio of 1.5. The cold wires were operated with constant current circuits built in-house, with a current of 0.1 mA. Wire diameters, lengths and separations are shown in figure 2. Fluctuating voltages from the constant temperature and constant current circuits were recorded on analogue FM tape and later digitized using an HP1000. Before digitizing, the voltages were low-pass filtered at a cut-off (−3 dB) frequency of 3.4 kHz. The sampling frequency f_s was 6.9 kHz while the record duration was 28 s.

The experimental methodology used in this paper requires comment and justification. The slight heating of the surface allows temperature to be used as a passive marker of the organized motion (see I). More specifically, two specific features of this motion, coolings and heatings, are marked by the temperature. To study the velocity field associated with these events, a desirable experimental

† The symbol A^+ is retained here as it has been used in I and in previous papers dealing with wall suction. However, it should not be confused with the van Driest parameter.

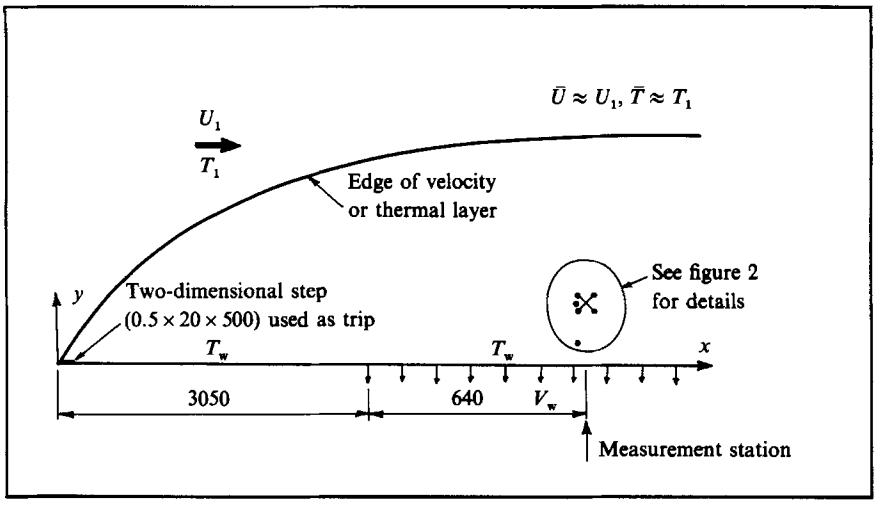

FIGURE 1. Sketch of experimental arrangement.

Quantity	Symbol	No suction	Suction
Boundary-layer thickness	δ (mm)	62	57
Displacement thickness	δ^* (mm)	8.1	6.2
Momentum thickness	δ_2 (mm)	6.1	4.9
Free-stream velocity	U_1 (m/s)	12.6	12.6
Friction velocity	U_τ (m/s)	0.48	0.67
Wall-suction velocity	V_w (m/s)	0	−0.037
Wall temperature (relative to free stream)	$T_w - T_1$ (K)	10	10
Friction temperature	T_τ (K)	0.42	0.55
Reynolds number	$R = U_1\delta_2/\nu$	5124	4116
Skin friction coefficient	c_f	32×10^{-4}	62×10^{-4}
Stanton number	St	16.7×10^{-4}	31×10^{-4}
Pressure gradient parameter	$\pi = (\delta^*/\rho U_\tau^2)\,\mathrm{d}P_1/\mathrm{d}x$	−0.019	+0.009
Wall-suction parameter	$A^+ = -V_w/U_\tau$	0	0.055

TABLE 1. Experimental conditions at the measurement station

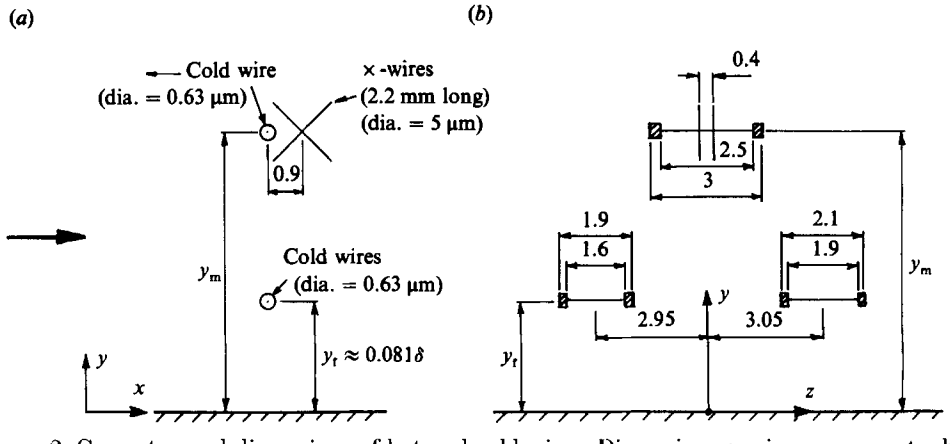

FIGURE 2. Geometry and dimensions of hot and cold wires. Dimensions are in mm, except where indicated.

arrangement would have been one where two components of velocity (necessitating therefore the use of an X-probe) as well as the scalar quantity are simultaneously measured at several points in space. Eight wires were used in the cold-wire array of I. Obviously, the investment in terms of equipment, data acquisition and processing would have been prohibitive had eight X-probes and eight cold wires been used. Although the use of a large number of X-probes has the obvious advantage of enabling the organized motion to be visualized from the instantaneous flow field (e.g. Antonia *et al.* 1988), useful conditional information can, in principle, be obtained with only one X-probe. In the present experiment, it was decided to use a single X-probe/cold-wire arrangement in combination with two cold wires, the latter being at a fixed distance from the wall (figure 2). Signals from the three cold wires would permit temperature fronts to be detected (detection details are given in the next section). The lateral spanwise displacement of the fixed cold wires, on either side of the X-probe/cold-wire arrangement, enabled the latter arrangement to be traversed so that the minimum distance to the wall from the centre of the X-probe is about 1 mm. This distance corresponds to $y^+ = 32$ for $A^+ = 0$ and $y^+ = 46$ for $A^+ = 0.055$. Rajagopalan *et al.* (1982) found that the spanwise separation at which the spanwise correlation of temperature first becomes negative is of order δ and independent of Reynolds number, provided $R \gtrsim 1500$. For $y_f = 5$ mm ($y_f/\delta = 0.081$ for $A^+ = 0$) the spanwise lengthscale is about 0.4δ. Since the chosen separation between the fixed cold wires is about 0.1δ, the correlation between the signals from the fixed cold wires should be sufficiently large for the purpose of detection.

3. Detection of organized motion

In I, coolings and heatings were detected by applying a modified VITA algorithm to temperature signals obtained simultaneously at several flow locations. A slightly different detection procedure is used in this investigation although we have drawn as much as possible, especially with regard to selecting detection parameters, on knowledge, obtained in I, about coolings and heatings (e.g. their lengthscale, average frequency and spatial inclination).

Here a procedure called WAG (window average gradient) is used to detect relatively sudden changes in temperature.† WAG can be applied to a signal obtained at one point in the flow or to signals simultaneously measured at different flow locations. In the present procedure, WAG was applied to the temperature signal obtained from the cold wire next to the X-probe (figure 1). It was also applied to the temperature signals obtained from the off-centreline cold wires (figure 1). WAG was preferred to VITA (variable interval time averaging) in the present work since the latter responds equally well to a large-scale heating/cooling and a burst of high-frequency signal, whereas the former filters out frequencies of period significantly shorter than the averaging window.

If we denote by θ_j the digital record of temperature fluctuations, where $j = 1, 2, \ldots, N$ (N = total number of data points; here $N = 192000$ corresponding to a record duration of 28 s), a value of WAG is calculated for a window of $(2\tau + 1)$ data points in the following manner

$$\mathrm{WAG} = \frac{\mathrm{sign}}{2\tau}\left(\sum_{i=j+1}^{j+\tau} \theta_i - \sum_{i=j-\tau}^{j-1} \theta_i\right), \tag{1}$$

† WAG was applied to lateral velocity fluctuations in the far-wake of a cylinder (Antonia *et al.* 1987*b*).

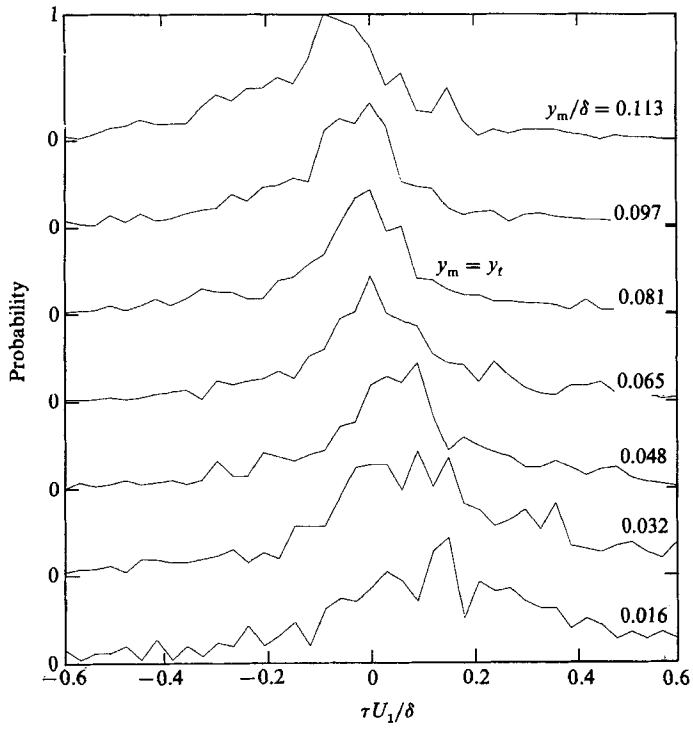

FIGURE 3. Relative probability of time delay between coolings detected at the moving cold wire (y_m/δ) and coolings detected at the fixed cold wires ($y_t/\delta = 0.081$). The origin $\tau = 0$ is the instant of detection at the fixed wires. $A^+ = 0$.

where the centre of the window is at $i = j$ and 'sign' is assigned a value of -1 when searching for coolings and $+1$ when searching for heatings. The window is moved point by point through the digital record and a detection is recorded for each continuous patch of signal for which the following conditions are satisfied:

(i) WAG $\geqslant \kappa\theta'$, when the window is centred on the first point of the patch (κ is a threshold value and θ' denotes the r.m.s. value of θ);

(ii) WAG > 0, when the window is centred on every point in the patch.

The value of j, denoted by j_m, say, for which WAG is largest over the signal patch corresponds to a detection instant. The size $(2\tau+1)$ of the window should be small compared with the average period between fronts but large compared with the duration over which the sharp temperature variation occurs. Antonia *et al.* (1982) estimated that the average streamwise length of a cooling is about 0.1δ when the momentum thickness Reynolds number exceeds 3000. In I, it was found that $\bar{T}_c$, the average period between coolings, which is smaller by about a factor of 2 than the average period between heatings, was in the range $8 \lesssim \bar{T}_c U_1/\delta \lesssim 7$ for $A^+ = 0$. In the present investigation, the size $(2\tau+1)$ of the window, normalized by U_1 and δ, was equal to 1.3 (for either heatings or coolings) when $A^+ = 0$ and 1.4 when $A^+ = 0.055$. As in I, κ was optimized by visually comparing the detection instants with the temperature traces. The final choices for κ were 0.6 and 0.5 for coolings and heatings respectively. The same values were used, with and without suction.

The application of the algorithm to the moving cold-wire signals yielded N_m detections. A multichannel version of the algorithm was applied to the two fixed wires, resulting in N_f detections, where N_f was about 62% of the number of

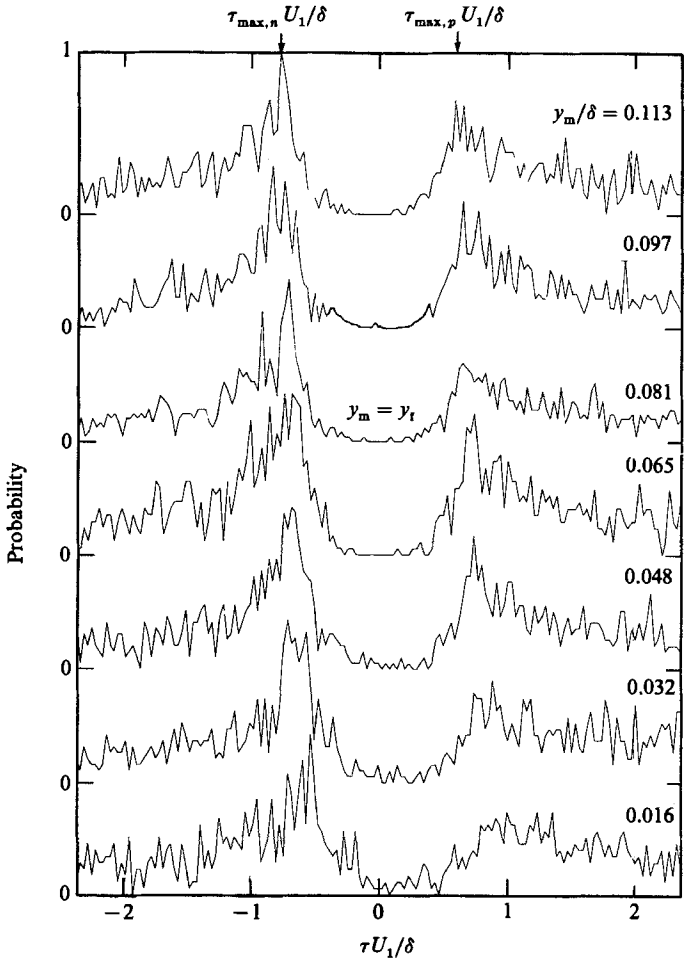

FIGURE 4. Relative probability of time delay between coolings detected at the moving cold wire (y_m/δ) and heatings at the fixed cold wires ($y_f/\delta = 0.081$). The origin $\tau = 0$ is the instant of detection at the fixed wires. $A^+ = 0$.

detections obtained from applying the single-channel algorithm to either one of the fixed wires. The final number of detections N_t was obtained by matching the moving-wire detections with the fixed-wire detections after allowing for the average inclination, in the (x, y)-plane, of coolings and heatings. To determine this inclination, the relative probability of the time delay between detections at the moving cold wire and detections at the fixed cold wires was calculated. The resulting distributions for coolings and $A^+ = 0$ are shown in figure 3 for several values of y_m. In figure 3 the time delay is referenced to the detection instant at the fixed wires ($y_f/\delta = 0.081$) and the maximum probability has been made equal to unity. It is evident that the time delay at which the maximum probability occurs is positive for $y_f/\delta \lesssim 0.081$ and negative for $y_f/\delta \gtrsim 0.081$. This corresponds to the cooling being detected at either later or earlier times relative to the fixed wires, depending on whether the moving wire is either nearer to or further from the wall, referenced to the fixed wires. The magnitude of $\tau_{max} U_1/\delta$, at which the probability is maximum, is in close agreement with that found in I on the basis of detections using a y-array of cold wires. Relative probabilities of time delays between heatings at the moving wire and heatings at the

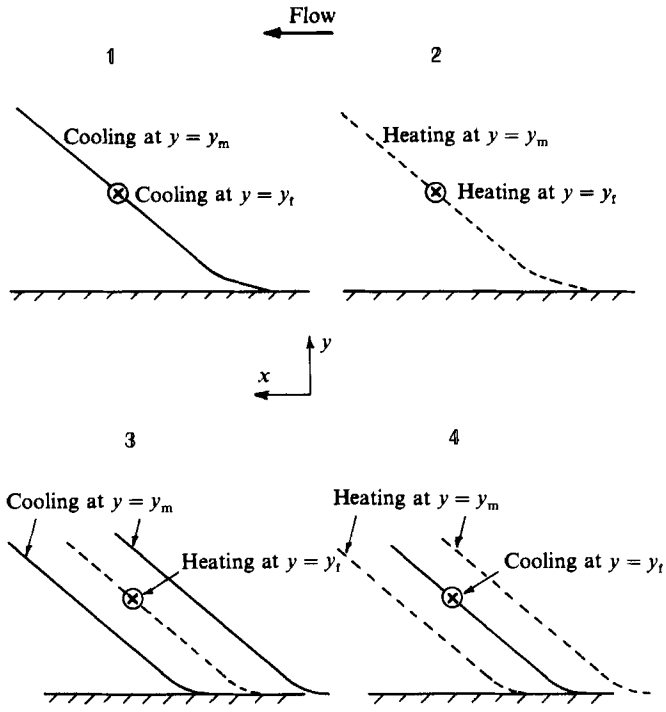

FIGURE 5. Schematic arrangement of the four detection configurations.

fixed wires were also calculated; they are not shown here as they are very similar to those in figure 3.

Inspection of temperature signals from the cold wires indicates that a heating is preceded and followed by coolings. The inverse situation, i.e. the occurrence of heatings shortly before and after a cooling, is also observed. To quantify these observations, the probability of the time delay between detected coolings (or heatings) at the moving wire and detected heatings (or coolings) at the fixed wires has been calculated. The resulting distribution normalized to a maximum value of unity, is shown in figure 4 for the case of coolings at position y_m relative to heatings at position y_f. The reference detection instant ($\tau = 0$) in figure 4 corresponds to the detection of a heating at $y = y_f$. Relatively well-defined local maxima occur at positive ($\tau_{max,p}$) and negative ($\tau_{max,n}$) values of the time delay τ. The maximum probability is larger at $\tau_{max,n}$ than at $\tau_{max,p}$, indicating that the cooling/heating combination is better defined than heating/cooling. When $y_m \approx y_f$, $\tau_{max,p} \approx |\tau_{max,n}|$. For $y_m > y_f$ and $y_m < y_f$, the relative magnitudes of $\tau_{max,p}$ and $\tau_{max,n}$ are consistent with the observed inclination of coolings with respect to the wall. The relatively slow decrease in the probability for $\tau > \tau_{max,p}$ or $|\tau| > |\tau_{max,n}|$ simply underlines the jitter that exists in the interval between coolings and heatings. Despite this, figure 4 implies a relatively unique spatial relationship between coolings and heatings. Distributions similar to those in figure 4 were obtained (but not shown here) when heatings are detected at the moving-wire location relative to a cooling at the fixed-wire location. In this case, the maximum probability is generally slightly larger at $\tau_{max,p}$ than at $\tau_{max,n}$, consistent with what has been inferred from figure 3.

The four different detection cases that have been studied are shown in figure 5. To obtain the final number N_t of detections, N_f was matched with N_m when the latter

occur within a narrow band centred on τ_{max}, for 1 and 2, and on both $\tau_{max,n}$ and $\tau_{max,p}$ for 3 and 4. For 1 and 2, the bandwidth around τ_{max} was typically $\pm 4\%$ of the average period between either heatings or coolings while for 3 and 4, the bandwidths centred on $\tau_{max,p}$ and $\tau_{max,n}$ were typically $\pm 8\%$. For 1 and 2, N_t is typically in the range 100–200 depending on y_m, whereas N_t varies between 25 and 50 for 3 and 4. Results have been obtained for all four cases, but are presented in more detail for 1 and 2 since these configurations are statistically more significant than 3 and 4.

4. Conditional and structural averaging

We consider here the digital time series corresponding to an instantaneous flow quantity $F_j (\equiv U, V$ or the instantaneous temperature $T)$ which comprises a total of N equi-spaced samples ($j = 1, \ldots, N$). The conditional average of F is defined as follows

$$\langle F \rangle_k = \frac{1}{N_t} \sum_{m=1}^{N_t} F_{j_m+k}, \tag{2}$$

where j_m is the value of j at the instant of detection and k, which may be positive or negative, represents the offset, relative to the instant of detection. N_t is the total number of detections.

As for the plane jet (Antonia *et al.* 1986) and plane wake (Antonia *et al.* 1987*a*) investigations, use is made of the triple decomposition to estimate the contribution that the organized motion makes to the Reynolds stresses and conventional heat fluxes. The instantaneous quantity F_{j_m+k} is written as

$$F_{j_m+k} = \bar{F} + \langle f \rangle_k + f_{s,j_m+k}, \tag{3}$$

where $\bar{F}$ is the global mean (the overbar denotes a conventional time average) and $\langle f \rangle$ is identified with the contributions from the organized large-scale motion. Antonia *et al.* (1986) referred to f_s as the random or incoherent fluctuation although it should be noted (e.g. Antonia *et al.* 1987*b*) that this description may not be entirely appropriate since it excludes the possibility that the fine structure can be spatially organized. In the context of a Reynolds decomposition, the difference $(F_{j_m+k} - \bar{F})$ represents the instantaneous fluctuation f_{j_m+k}, so that

$$f_{j_m+k} = \langle f \rangle_k + f_{s,j_m+k}.$$

When the previous relation is conditionally averaged, using (2), we obtain

$$\langle f_{j_m+k} \rangle = \langle f \rangle_k$$

with the assumption that $\langle f \rangle$ and f_s are uncorrelated, i.e. with $\langle f_s \rangle \equiv 0$. For products which involve two fluctuations f and g (like f, g stands for either u, v or θ), we can write

$$\langle fg \rangle_k = \langle f \rangle_k \langle g \rangle_k + \langle f_s g_s \rangle_k. \tag{4}$$

An average contribution of the organized motion to $\overline{fg}$, can be obtained by averaging $\langle fg \rangle$ over the mean period of the motion. We refer to this type of averaging as structural averaging and denote it by a tilde

$$\widetilde{\langle fg \rangle} = \frac{1}{2k_1 + 1} \sum_{-k_1}^{k_1} \langle fg \rangle_k, \tag{5}$$

the averaging duration extending k_1 samples on either side of the detection instant. It follows from (4) and (5) that

$$\widetilde{\langle fg\rangle} = \widetilde{\langle f\rangle\langle g\rangle} + \widetilde{\langle f_s g_s\rangle}. \tag{6}$$

Strictly, the left-hand side of (6) is equal to $\overline{fg}$ when all the samples in the original digital time series for F and G are used in forming $\langle fg\rangle$ (Antonia *et al.* 1986). In this case, the first term on the right-hand side of (6) represents the contribution from the organized motion to $\overline{fg}$.

5. Conditional velocity vectors, spanwise vorticity and strain rate

Once conditionally averaged velocities $\langle u\rangle$ and $\langle v\rangle$ are obtained by the averaging procedure described in the previous section, it is possible to 'construct' the velocity vector field associated with coolings and heatings in the (x, y)-plane. Assumptions needed for this construction are discussed below.

It has been pointed out (e.g. Brown & Thomas 1977; Thomas 1977*a*, *b*; Coles 1982, 1984; Hussain 1983, 1986; Antonia *et al.* 1987*a*) that the flow organization is evident only when it is viewed in a suitably moving frame of reference. In general, the choice of convection velocity $\bar{U}_c$ for this reference frame is not straightforward. Perry & Chong (1987) noted that it is difficult to define this convection velocity precisely since it is likely that different parts of the organized motion are convected at different velocities. In the case of the boundary layer, it is unrealistic to expect the organized motion to travel with a unique convection velocity; in this context, there is sufficient experimental evidence to indicate a dependence of $\bar{U}_c$ on y, the distance from the wall. To view the organized motion in a turbulent boundary layer, Brown & Thomas (1977) used the convection velocity ($\equiv 0.8U_1$) of the low-frequency component of the wall pressure fluctuation. In I, convection velocities of coolings and heatings were determined by different methods: transit time, phase- and space-correlation as applied to temperature signals obtained from an array of cold wires aligned in the x-direction. Although there were quantitative differences, all methods yielded the same qualitative distribution with a local maximum within the buffer layer. The distributions of $\bar{U}_c/U_1$, which are shown in figure 6 for $y/\delta \lesssim 0.4$, were obtained by the transit time method. Mean velocity distributions are also shown in this figure. Ignoring the local maximum in $\bar{U}_c$ in the buffer layer and the slight rate of increase of $\bar{U}_c/U_1$ for $y/\delta \gtrsim 0.02$, we have assumed a constant value of $\bar{U}_c/U_1$, 0.67 for $A^+ = 0$ and 0.79 for $A^+ = 0.055$. This choice ignores that coolings have a slightly higher convection velocity than heatings but accounts for the observed increase in convection velocity due to suction. The chosen values, indicated by the heavy lines in figure 6, are reasonable approximations in the range 0.05δ–0.15δ.

To view the organized motion, it is important that the conditional data are positioned in the (x, y)-plane correctly. Since the main interest is in flow patterns relative to coolings and heatings, any point on a cooling or heating could be used as a reference location. Here, we use $y = y_f$. At other values of y, the detection instant is delayed, relative to that at y_f, by an amount equal to the delay τ_{max} at which the relative probability of finding a cooling or heating at the moving cold wire relative to the fixed-wire detections is a maximum (i.e. figure 3 for coolings at both y_m and y_f or figure 4 for coolings at y_m relative to a heating at y_f). This time delay is converted to a streamwise separation with the transformation $\Delta x = -U_t \tau_{max}$. This latter relation requires another velocity U_t to be specified. One possibility is to use Taylor's hypothesis, i.e. $U_t \equiv \bar{U}$, but there are shortcomings with this assumption

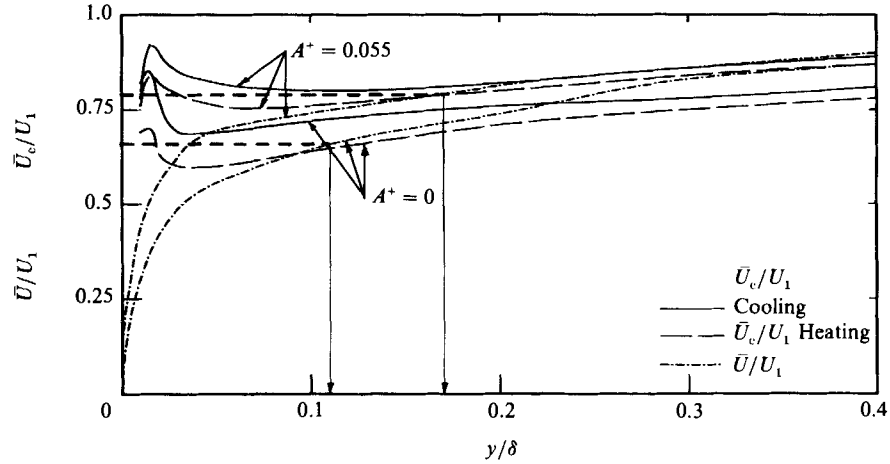

FIGURE 6. Convection velocities of coolings and heatings for $A^+ = 0$ and $A^+ = 0.055$. Mean velocity profiles are also shown. The assumed values of $\bar{U}_c/U_1$ (0.67 for $A^+ = 0$ and 0.79 for $A^+ = 0.055$) are shown by heavy horizontal lines.

(e.g. Hussain 1983, 1986). Thomas & Brown (1977) used U_1 but, again, it would be difficult to defend such an assumption. Here, U_t is taken equal to $\bar{U}_c$. In general, there is no *a priori* reason to identify U_t with $\bar{U}_c$. However, in the present flow, the spatial relationship between coolings and heatings, emphasized in parts 3 and 4 of figure 5, and the small difference between convection velocities of heatings and coolings provide some justification for replacing U_t by $\bar{U}_c$.

In figure 7, the inclination of each vector to the horizontal is equal to

$$\tan^{-1}[(\langle v\rangle + \bar{V})/(\bar{U} + \langle u\rangle - \bar{U}_c)]$$

while the length of each vector is

$$[(\bar{U} + \langle u\rangle - \bar{U}_c)^2 + (\langle v\rangle + \bar{V})^2]^{\frac{1}{2}}.$$

The normal mean velocity $\bar{V}$ was calculated from $\bar{U}$ and the continuity equation ($\bar{V}$ is negligible from $A^+ = 0$ but becomes important close to the wall for $A^+ = 0.055$). To avoid confusion, arrowheads are not shown but there is only minimum ambiguity since the origin of each vector corresponds to the value of y at which the measurement is made. The actual values of y at which measurements were made are denoted by the horizontal arrows on the side of figure 7 (a). At other y values, the data were obtained by interpolation.

The velocity vectors plotted in figure 7 are seen in a translating frame of reference (in this frame, the wall moves to the right at a velocity $-\bar{U}_c$). For ease of viewing, the vertical scale has been exaggerated (by a factor of 3) relative to the horizontal scale.

Salient features in figure 7 are the lines defined by the coolings and the rotational patterns which the vectors delineate on either side of these lines. The conspicuousness of the lines is not surprising since coolings are associated with sudden changes in temperature (or velocity) and the detection in figure 7 focuses, either directly (e.g. figures 7 a, b) or indirectly (e.g. figures 7 c, d) on this feature. The occurrence of the rotational patterns is somewhat surprising especially since they appear to be centred on the reference location of heatings (e.g. figures 7 c, d).

Two types of critical points (the velocity components are zero at these points) can

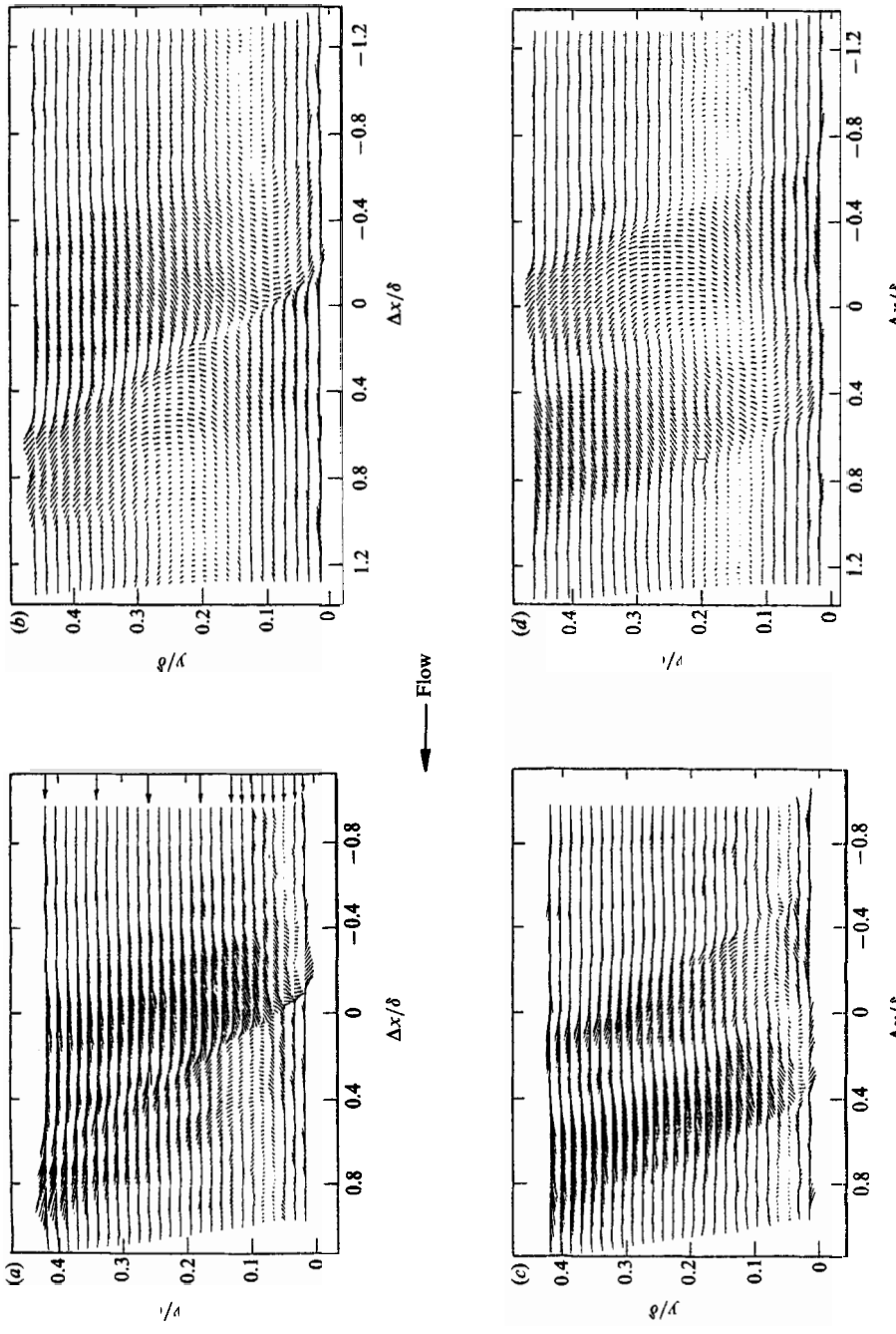

FIGURE 7. Velocity vectors associated with coolings and heatings. The frame of reference translates in the flow direction with a velocity $\bar{U}_c$. The origin $\Delta x = 0$ is the detection instant at $y = y_t$. Coolings, case 1: (*a*) $A^+ = 0$; (*b*) $A^+ = 0.055$; Heatings, case 2: (*c*) $A^+ = 0$; (*d*) $A^+ = 0.055$.

be recognized in figure 7: saddles and foci. The coolings are directed along the diverging separatrices through the saddle points whereas heatings go through foci. The ordinates of these points are given approximately by the values of y/δ for which $\bar{U}_c \approx \bar{U}$; these values are identified by the arrows in figure 6. Strictly, one should use the convection velocity of coolings for saddle points and that of heatings for foci but, as noted earlier, the difference is small. For our choice of $\bar{U}_c/U_1$ (figure 6), the critical point ordinates should occur at approximately 0.11δ for $A^+ = 0$ and 0.18δ for $A^+ = 0.055$. Figure 7 provides qualitative support for this difference.

It is possible to construct sectional streamlines, as defined by Perry & Chong (1987), using the data of figure 7, even though these data are for a two-dimensional cut through a three-dimensional flow field. These streamlines have been determined by numerically integrating the velocity data and their tangency to the velocity vectors is generally satisfactory. The discontinuities in the sectional streamlines (figures 8 and 9) are primarily due to the discretization of the velocity data and its interaction with the algorithm used; the latter attempts to calculate the continuation of a streamline across a full grid spacing in a single step, and occasionally fails. The data points cannot be more closely spaced because of experimental limitations.

The sectional streamlines in figure 8, which correspond to cases 1 and 2, highlight the nature of the critical points more effectively than the vector plots of figure 7. In particular, the centres of the rotational patterns can be identified with unstable foci when heatings are detected (figures 8*c*, *d*). These foci are less clearly defined when coolings are detected (figures 8*a*, *b*). This is not true however in case 4 (figures 9*a*, *b*) where the degree of organization is greater than in case 2 (figures 8*a*, *b*). Similarly, diverging separatrices and saddle points on either side of heatings are defined more clearly in figure 9(*c*, *d*) than in figure 8(*c*, *d*).

Figures 7, 8 and 9 are a good illustration of how the flow organization is increased by suction. The longitudinal and lateral scales of the flow patterns are greater for $A^+ = 0.055$ than for $A^+ = 0$. Near the wall, the streamwise variation in the pathline curvature (figures 8 and 9) is more gradual for $A^+ = 0.055$ than $A^+ = 0$. Note that an increase in $\bar{U}_c$ would raise the locations of the critical points in figures 7, 8, 9 but the relative behaviour of patterns between $A^+ = 0$ and $A^+ = 0.055$ would not be affected.

Approximations to the conditional spanwise vorticity $\langle \Omega \rangle$ and the conditional strain rate $\langle S \rangle$, where

$$\langle \Omega \rangle = \frac{\partial \langle V \rangle}{\partial x} - \frac{\partial \langle U \rangle}{\partial y}, \tag{7}$$

and

$$\langle S \rangle = \frac{\partial \langle V \rangle}{\partial x} + \frac{\partial \langle U \rangle}{\partial y}, \tag{8}$$

have been calculated, with the first term on the right-hand sides of (7) and (8) estimated using the space–time transformation $\partial/\partial x = -\bar{U}_c^{-1}\partial/\partial t$.

Contours of $\langle \Omega \rangle$ associated with coolings, case 1, and heatings, case 2, are shown in figure 10. An interesting feature of figure 10 is the manner in which the contours are stretched in the direction of the cooling. For clarity, only a few contours are presented but the same contour values, normalized using U_1 and δ, are used for $A^+ = 0$ and $A^+ = 0.055$. The largest values of $\langle \Omega \rangle$ occur near the wall,† as expected, but the absence of significant vorticity near the focus was not anticipated. Although

† The low-frequency variation of $\langle \Omega \rangle$ near the wall reflects the low-frequency change in the wall shear stress, established in previous investigations (e.g. Brown & Thomas 1977; Rajagopalan & Antonia 1979).

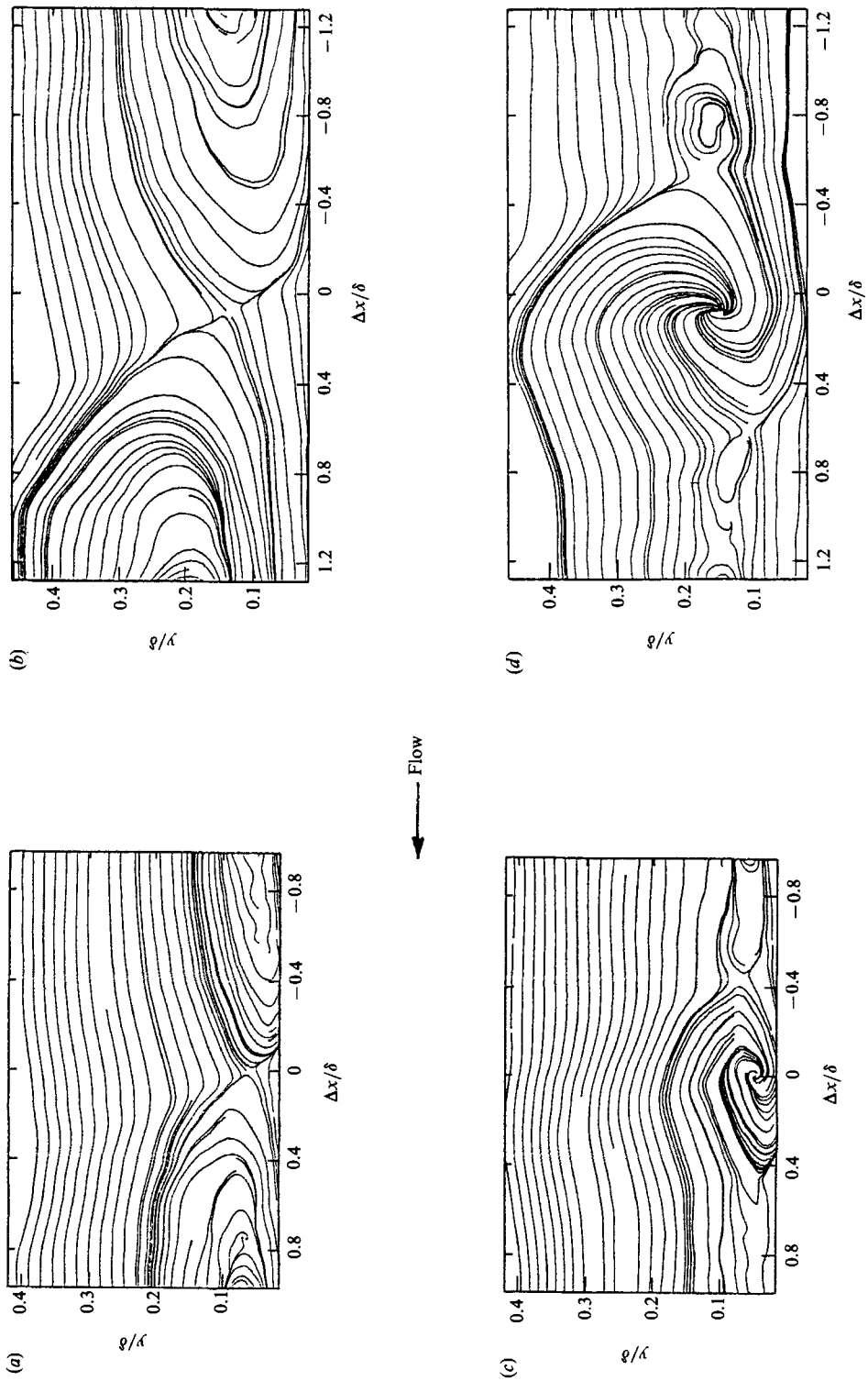

FIGURE 8. Sectional streamlines associated with coolings and heatings. The frame of reference translates in the flow direction with a velocity $\bar{U}_e$. Coolings, case 1: (*a*) $A^+ = 0$; (*b*) $A^+ = 0.055$; Heatings, case 2: (*c*) $A^+ = 0$; (*d*) $A^+ = 0.055$.

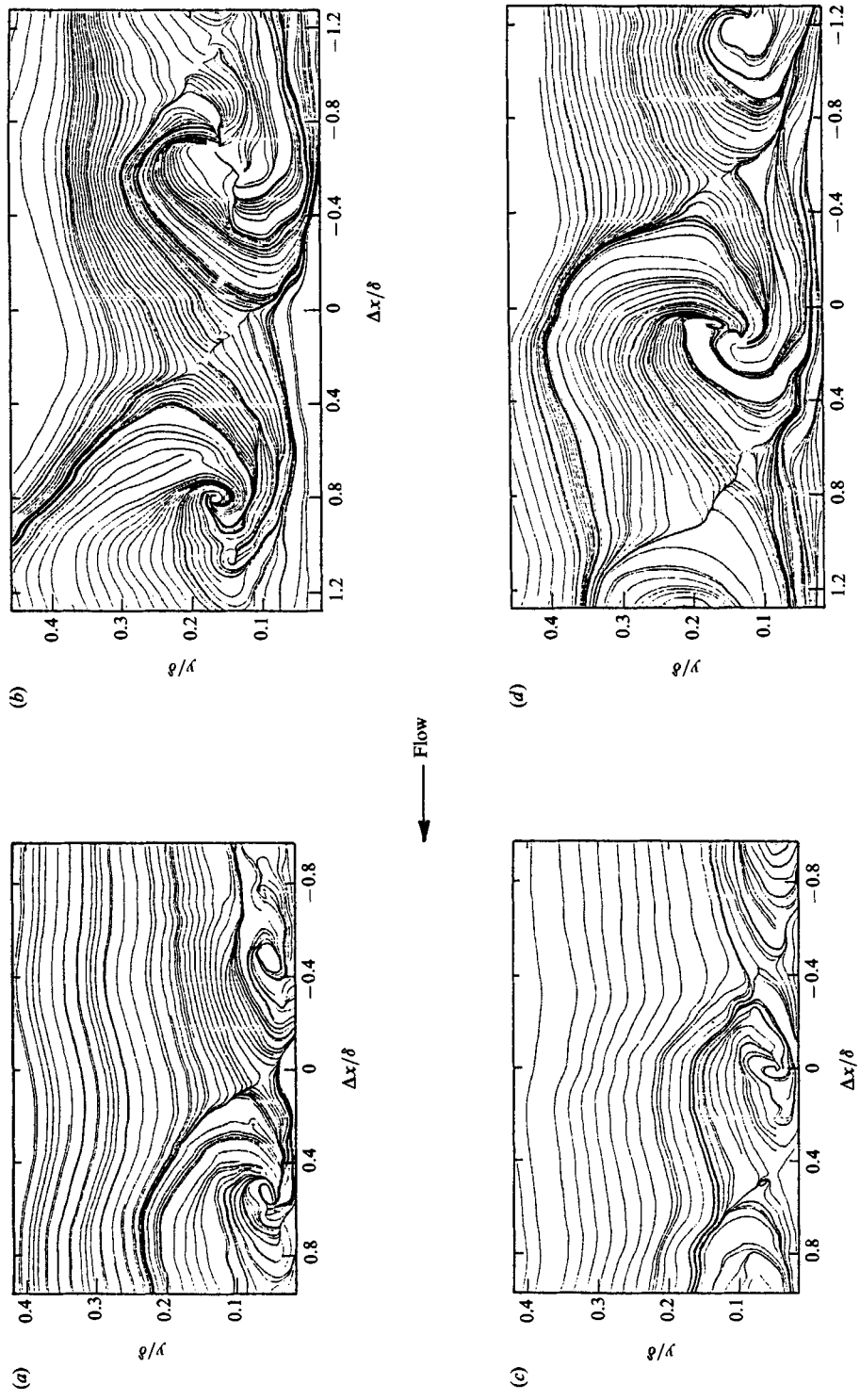

FIGURE 9. Sectional streamlines associated with combinations of coolings and heatings. The frame of reference translates in the flow direction with a velocity $\bar{U}_c$. Heatings at y_m, cooling at y_f, case 3: (*a*) $A^+ = 0$; (*b*) $A^+ = 0.05$; Coolings at y_m, heating at y_f, case 4: (*c*) $A^+ = 0$; (*d*) $A^+ = 0.05$.

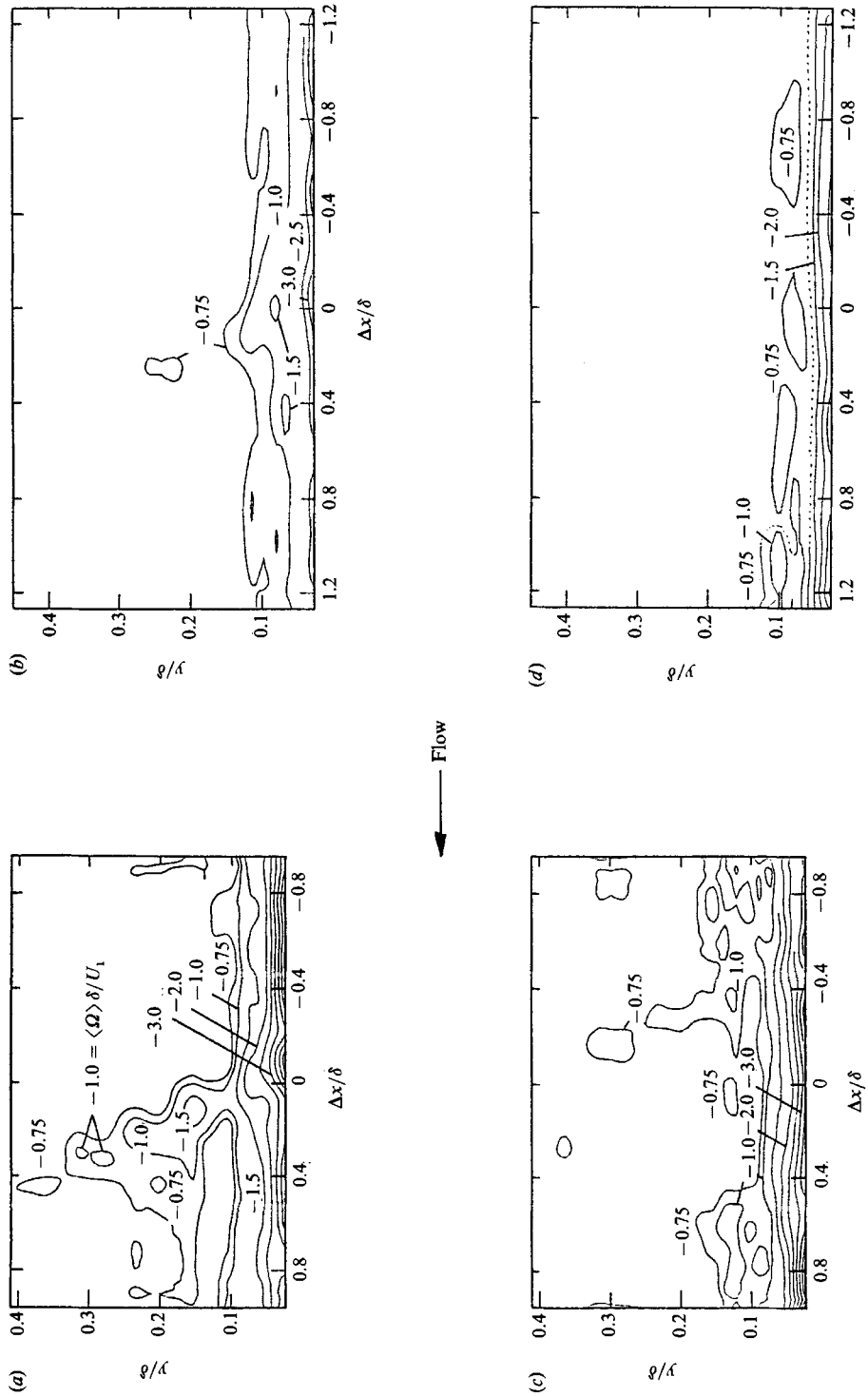

FIGURE 10. Contours of conditional spanwise vorticity $\langle\Omega\rangle\delta/U_1$ associated with coolings and heatings. Coolings, case 1: (*a*) $A^+ = 0$; (*b*) $A^+ = 0.055$; Heatings, case 2: (*c*) $A^+ = 0$; (*d*) $A^+ = 0.055$.

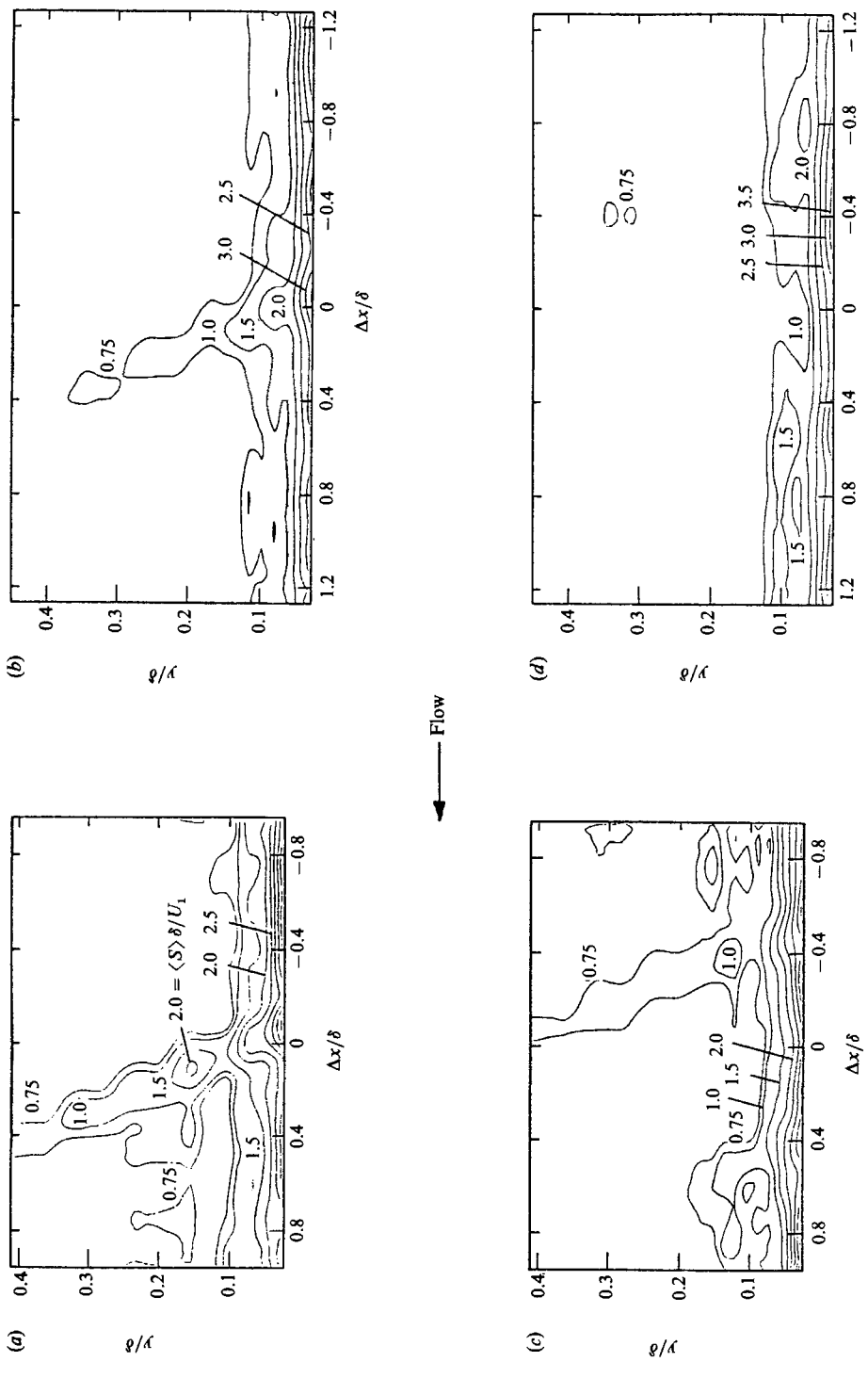

FIGURE 11. Contours of conditional strain rate $\langle S\rangle\delta/U_1$ associated with coolings and heatings. Coolings, case 1: (*a*) $A^+ = 0$; (*b*) $A^+ = 0.055$; Heatings, case 2: (*c*) $A^+ = 0$; (*d*) $A^+ = 0.055$.

$\langle\Omega\rangle$ is not negligible at the focus, the largest concentration resides along the cooling. Relative to figures 10(*a*) and 10(*c*), the contours in figures 10(*b*) and 10(*d*) are stretched away from the wall and the largest $\langle\Omega\rangle$ contours are flattened near the wall. When the detection is based on heatings, the contours remain stretched along coolings on either side of heatings. This effect is more evident in figure 10(*c*) than in figure 10(*d*) although the curvature of the contours (figure 10(*d*)) nearest the wall suggests that the largest vorticity concentration does not lie below the focus but on either side of the focus, approximately where coolings leave the wall. Large values of $\langle S\rangle$ occur mainly along coolings (figure 11) regardless of whether the detection is based on coolings or heatings. Vorticity and strain rate contours, not shown here, for cases 3 and 4 simply emphasize the stretching along coolings.

6. Implications with respect to the flow structure

The flow patterns associated with coolings have several features in qualitative agreement with the streamline patterns which Thomas (1977*a*, *b*) and Thomas & Brown (1977), collectively referred to as TB in this section, obtained for the organized motion in a turbulent boundary layer at a relatively large Reynolds number ($R \approx 10000$). Before we discuss these features in the context of the flow structure, it should be pointed out that TB did not calculate streamlines but sketched them in as visual approximations to streamlines. More importantly, the detection procedure used by TB differs from the present one in that it was based on the steep velocity gradients which are assumed to occur on the upstream surface of the large structure. More specifically, their detection focused on the rectified high-frequency component of the u velocity signal. As such it did not discriminate between positive and negative gradients and therefore weighted both coolings (or accelerations, $\partial U/\partial t > 0$) and heatings (or decelerations, $\partial U/\partial t < 0$). That the resulting conditional averages only indicate a temporal increase in $\langle U\rangle$ suggests that coolings dominate (alternately, the back of the structure is important, the interpretation given by TB) but it can also be argued that the inclusion of the decelerations could have degraded the velocity field associated with the back of the structure.†

The TB streamlines indicate a saddle point at $y/\delta \approx 0.25$; the difference between this location and the present saddle point location may be due to the difference in the choice of $\bar{U}_c$ ($0.8U_1$ for TB compared with $0.67U_1$ here). Upstream of the separatrix (or the back of the structure), the TB streamlines imply the presence of a weak recirculating pattern centred at about the same distance from the wall as the saddle point. This feature is also evident in the vector patterns of figure 7. Downstream of the separatrix, TB sketched in a recirculating region which extends outwards to the edge of the layer but the centre of this region is in fact not much above the saddle point. As noted earlier, the present patterns indicate a recirculating region closer to the wall although the present information only extends to $y/\delta \simeq 0.4$. TB interpret their region as reflecting the vorticity of the large-scale bulges. This feature can be emphasized further if one chooses a frame of reference that travels with the upper part of the bulges. This is precisely the result obtained by Blackwelder & Kovasznay (1972) and Falco (1977) using measurements and flow visualizations respectively in the outer intermittent region of the layer. One expects the topology in the outer part

† It is possible that TB's use of bootstrapping (or correlation to conditional average procedure) may have eliminated the decelerations.

of the boundary layer to be qualitatively similar to that obtained in the self-preserving wake (e.g. Antonia *et al.* 1987*a*).

The discussion in I suggested a likely association between coolings and hairpin vortices. The results of figures 7 to 11 provide partial support for this suggestion. Hairpin vortices, as observed for example in the flow visualizations of Head & Bandyopadhyay (1981), extend to different distances from the wall. This observation appears consistent with the wall similarity requirement that motions responsible for turbulent transport should have lengthscales proportional to distance from the wall (e.g. Townsend 1987). The concentration of spanwise vorticity should occur at the tips of the vortices and therefore vary uniformly with y. If these vortices are captured by the present detection scheme, the conditional averaging procedure should result in the spanwise vorticity contours being coincident with the strain rate contours. This is indeed what is observed.

Perry & Chong (1982) have modelled the turbulent boundary layer by an agglomeration of hairpin or Λ vortices and found that these vortices have the correct transport properties. Using the Biot–Savart law, these authors calculated the flow field due to an isolated Λ vortex and its image in the wall. Relative to an observer moving with the convection velocity of the vortex, the calculated velocity field indicated a stable focus at the head of the vortex with a saddle located immediately below this focus. As noted above, the present flow topology is best interpreted as the flow field due to an ensemble of hairpin vortices each of which may have been stretched out to different distances from the wall. In this context, it seems unlikely that the unstable foci in figures 8 and 9 are directly comparable with the flow field calculated for an isolated Λ vortex.

TB noted that streamlines immediately downstream of the separatrix and close to the wall display a convex curvature and suggested that this curvature was sufficient to produce a Taylor–Görtler type of instability. An approximate model of this rotational instability yielded reasonable order of magnitude estimates of the spanwise spacing of low-speed streaks. They also suggested that this rotational instability was more likely to be responsible for the bursting sequence than the convected pressure field associated with the large structure. The convex nature of the near-wall pathlines immediately downstream of the coolings can be observed in figures 8 and 9. Suction reduces this curvature, as can be seen by comparing the near-wall regions of figures 8(*a*) and 8(*b*). This decrease appears consistent with the stabilizing influence of suction on the near-wall region.

7. Contribution to the conventional velocity and temperature variances and fluxes

To quantify the importance of the organized motion associated with coolings and heatings in the context of the quantities $\overline{u^2}$, $\overline{v^2}$, $\overline{\theta^2}$, $\overline{uv}$, $\overline{u\theta}$ and $\overline{v\theta}$, conditional averages $\langle fg\rangle_k$, $\langle f\rangle_k$, $\langle g\rangle_k$ were first calculated in the manner described in §4. To determine structural averages, using (5), a value of k_1 needs to be selected. This selection is not as straightforward in the boundary layer as in free shear flows such as the plane jet or the plane wake. In these latter flows, the average wavelength of the organized motion is known with reasonable accuracy. It is recognized that the boundary-layer flow is less organized: a reflection of this may be the large range of values reported for the average wavelength of the bursting cycle (e.g. Fleischmann & Wallace 1984; Bogard & Tiederman 1986). Since the primary interest here is not in the absolute value of the contribution from the organized motion but in its importance relative to

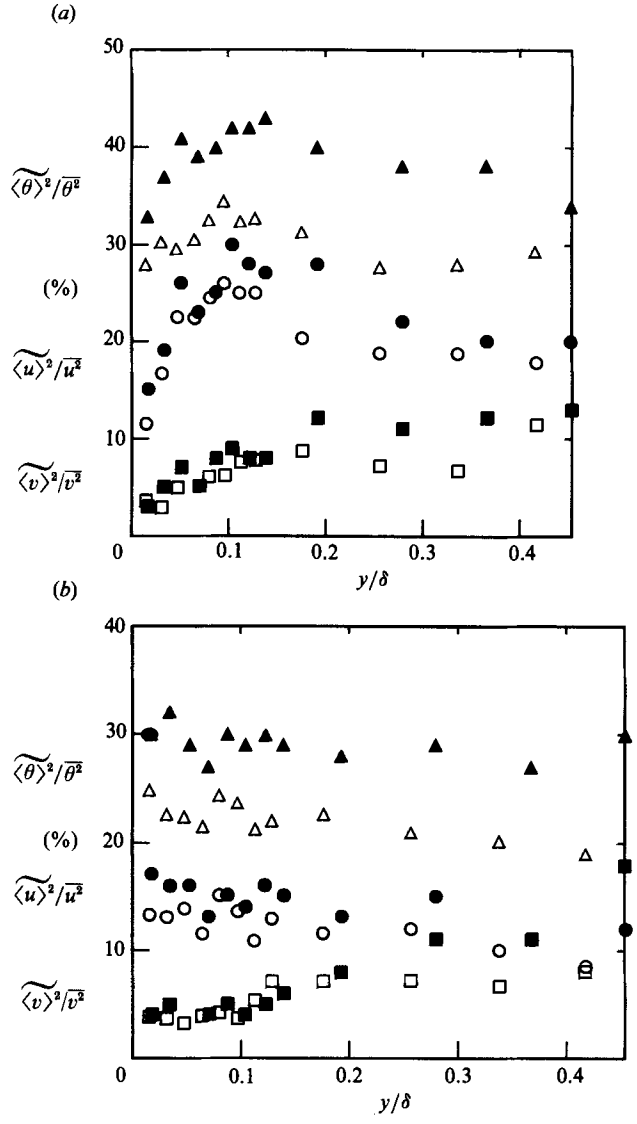

FIGURE 12. Relative contributions of organized motion associated with coolings and heatings to the conventional variances. ○, $\widetilde{\langle u\rangle^2}/\overline{u^2}$; □, $\widetilde{\langle v\rangle^2}/\overline{v^2}$; △, $\widetilde{\langle\theta\rangle^2}/\overline{\theta^2}$. (*a*) Coolings, case 1; (*b*) heatings, case 2. Open and filled in symbols are for $A^+ = 0$ and $A^+ = 0.055$ respectively.

the conventional quantities, namely in the ratio $\widetilde{\langle f\rangle\langle g\rangle}/\overline{fg}$, k_1 was selected to correspond to a streamwise distance† of $\pm\delta$ (relative to the detection point) for both $A^+ = 0$ and $A^+ = 0.055$. This distance corresponds approximately with the most probable distance between consecutive coolings as illustrated in figure 4. In view of the relatively small number of detections (typically 100–200 for cases 1 and 2), only about 5–10% of the total record duration was used in forming the structural averages. Nevertheless, the value of $\widetilde{\langle fg\rangle}$, equation (6), was found to be in reasonable agreement with that of $\overline{fg}$, suggesting that the parts of the record which have been selected are representative of the whole record. For example, for case 1, the ratios

† The convection velocity $\bar{U}_c$ was used for the time–space conversion.

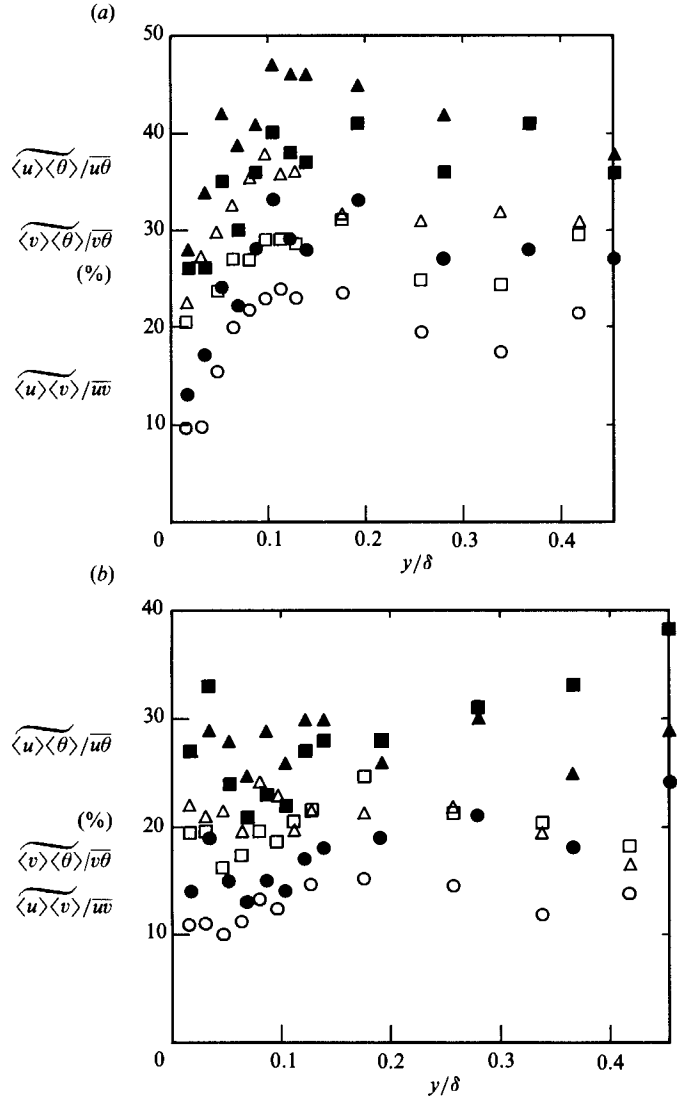

FIGURE 13. Relative contributions of organized motion associated with coolings and heatings to the Reynolds shear stress and the longitudinal and normal heat fluxes. ○, $\widetilde{\langle u\rangle\langle v\rangle}/\overline{uv}$; □, $\widetilde{\langle v\rangle\langle\theta\rangle}/\overline{v\theta}$; △, $\widetilde{\langle u\rangle\langle\theta\rangle}/\overline{u\theta}$. (*a*) Coolings, case 1; (*b*) heatings, case 2. Open and filled in symbols are for $A^+ = 0$ and $A^+ = 0.055$ respectively.

$\widetilde{\langle uv\rangle}/\overline{uv}$ and $\widetilde{\langle v\theta\rangle}/\overline{v\theta}$ are equal to 0.93 and 1.13 respectively for $y/\delta = 0.05$ and $A^+ = 0$; the corresponding values at $y/\delta = 0.13$ are 0.98 and 1.11. The departure from unity of these ratios is sufficiently small, given the experimental uncertainty (of order $\pm 6\%$ and $\pm 8\%$ for $\overline{uv}$ and $\overline{v\theta}$ respectively),† to assume that $\langle fg\rangle \approx \overline{fg}$.

The ratio $\widetilde{\langle f\rangle\langle g\rangle}/\overline{fg}$, with $f = g$ ($\equiv u$, v or θ) is plotted in figure 12(*a*) for case 1 and figure 12(*b*) for case 2. Three main points can be made:

(i) This ratio is largest for θ (the maximum is of order 0.4 for $A^+ = 0.055$) and

† The measured distributions, not shown here, of $\overline{uv}/U_1^2$ and $\overline{v\theta}/U_1(T_w - T_1)$ are in close agreement with the measurements, with approximately the same experimental conditions, reported in Fulachier (1972) and Fulachier *et al.* (1977).

smallest for v (typically less than 0.1). A corollary of this is that the 'random' contribution to the temperature variance and the normal stress, especially $\overline{v^2}$, cannot be ignored.

(ii) The ratio is larger for coolings than heatings except near the wall where contributions from heatings and coolings are comparable. The contribution from coolings increases away from the wall up to $y/\delta \approx 0.1$, in contrast with the negligible variation for heatings.

(iii) There is a significant increase due to suction, the increase tending to be more important for temperature than for velocity.

The above comments apply equally well to contributions (figure 13a, b) to the conventional shear stress and heat fluxes. Note that the ratio $\langle\widetilde{v}\rangle\langle\widetilde{\theta}\rangle/\overline{v\theta}$ is larger than $\langle\widetilde{u}\rangle\langle\widetilde{v}\rangle/\overline{uv}$, implying that the organized motion (hairpin vortices) is more efficient at transporting heat than momentum. A similar result has been inferred from measurements in free shear flows, for example by Antonia *et al.* (1986) for a plane jet and Browne, Antonia & Bisset (1986) for a plane wake.

The effect of suction observed in figures 12 and 13 seems consistent with the findings in I and the increased topological organization (e.g. figures 7, 8 and 9) caused by suction. It should be recalled however that figures 12 and 13 give an indication of the relative importance of $\langle\widetilde{f}\rangle\langle\widetilde{g}\rangle$ and (indirectly) $\langle\widetilde{f_s g_s}\rangle$ with respect to $\overline{fg}$ rather than insight into how $\overline{fg}$ is produced. It was pointed out in I that the increased stabilization, due to suction, in the near-wall region is accompanied by a significant reduction in the number of coolings and heatings and a consequent decrease in $\overline{fg}$.

8. Concluding remarks

The present results permit a relatively unambiguous interpretation of coolings and heatings, the characteristics of which were obtained in a previous study (Antonia *et al.* 1987*a* or I). Relative to an observer travelling at an appropriate convection velocity, the topology of the boundary layer, over a region which extends from the wall to $y/\delta \approx 0.4$, indicates a succession of critical points: saddles and unstable foci. Coolings are aligned along diverging separatrices which go through the saddle points whereas heatings go through the foci, the latter occurring at the centre of regions bounded by coolings. Coolings are associated with a large strain rate and a large spanwise vorticity in contrast with the small strain rate and vorticity at the foci. The present evidence provides partial support for the association, suggested in I, between coolings and hairpin vortices. More definitive support would require three dimensional data on the topology, especially simultaneous information of the spanwise vorticity and either the normal or streamwise vorticity. From the point of view of contributions to Reynolds stresses, temperature variance and conventional heat fluxes, coolings are more important than heatings and transport heat more effectively than momentum.

The relatively small wall suction rate significantly increases the topological organization, as reflected in the increase of the space occupied by the organized flow patterns. Near the wall, the effect of suction is to reduce the magnitude of spanwise vorticity, strain rate and streamline curvature. As shown in I, the streamwise length of low-speed streaks is increased by suction although their average spanwise spacing (in wall units) is unaffected. The increase in the length of streaks is consistent with the increase in lengthscale, inferred by Dumas (1962) from spectra of u measured near the wall. All the previously discussed features are consistent with the stabilizing influence of wall suction and possibly the larger influence near the wall of the outer

eddies. Also consistent with the increased organization of the flow topology is the increase in the relative contribution of the organized motion to the conventional stresses, temperature variance and heat fluxes. It should be recalled however that the magnitudes of $\overline{uv}$ and $\overline{v\theta}$ are smaller with suction than without suction (e.g. Fulachier 1972; Fulachier *et al.* 1977), reflecting the suction caused decrease, as established in I, in the average frequency of coolings. There is, of course, a large negative shear stress gradient in the inner region when wall suction is applied (simply because of the boundary condition $\partial\tau/\partial y = V_w \partial\bar{U}/\partial y$ and the latter must be negative and maximum at the wall; in this sense, the effect of suction is fundamentally different to the case of no suction because of the importance of the inertia term $V_w \partial\bar{U}/\partial y$ at the wall). This case is somewhat similar to that which results from the imposition of a favourable pressure gradient (near the wall $\partial\tau/\partial y \approx \rho^{-1}\partial p/\partial x$) and it is therefore not surprising that in both cases there is a stabilizing influence on the near-wall flow. As mentioned in I, Kline *et al.* (1967) found that low-speed streaks tended to be stabilized by a favourable pressure gradient in much the same manner as low-speed streaks are stabilized by suction.

Although the effect of suction, as described in the preceding paragraph, is important in the context of flow topology and magnitudes of turbulence intensities, Reynolds shear stresses, temperature variances and heat fluxes, the effect on turbulence structure parameters does not seem significant. For example, Fulachier (1972) found that the correlation coefficient between u and v is practically unaffected by moderate suction, as are the turbulence structure parameters $a_1 = -\overline{uv}/(\overline{u^2}+\overline{v^2}+\overline{w^2})$ and $a_\theta = \overline{v\theta}/[\overline{\theta^2}^{\frac{1}{2}}(-\overline{uv})^{\frac{1}{2}}]$. However, it was also found (Dekeyser, Fulachier & Verollet 1977) that the anisotropy of the Reynolds stress tensor is increased by suction, which is consistent with the enhancement of the low-frequency part of the velocity and temperature spectra when suction is applied (Fulachier 1972). The present observed change to the flow topology due to suction is consistent with an increased anisotropy of the large-scale motion.

Any connection between the topology of the organized motion and the mean velocity profile can only be speculative unless a model is proposed for this motion. Perry & Chong's (1982) model, developed for an impervious smooth surface which assumes A vortices that are geometrically similar and have the same characteristic velocity scale, yields the mixing length relation $l = (-\overline{uv})^{\frac{1}{2}}/(\partial\bar{U}/\partial y) = \kappa y$. The flow topological evidence of the present paper and the flow visualizations of I do not preclude the validity of the assumption in Perry & Chong's model to the case of suction so that the mixing length relation should not be affected in the inner region. In the outer region, the present topological differences between suction and no suction reflect changes in lengthscales rather than changes in structure and are not necessarily inconsistent with the relatively weak differences between mean velocity profiles in the two flows. They are consistent with the increase in l (about 30% larger for $A^+ = 0.055$ than without suction) obtained by Verollet (1972), in the outer layer.

We are especially grateful to Dr L. V. Krishnamoorthy for his assistance with both experiments and computations, to Mr T. Benabid and Dr F. Anselmet for their contributions to the experiments, and to Mr D. K. Bisset for his assistance with computations. The support of the Australian Research Grants Scheme is gratefully acknowledged.

REFERENCES

ANTONIA, R. A., BISSET, D. K., BROWNE, L. W. B. & FULACHIER, L. 1987*a* *J. Fluid Mech.* **184**, 423–444.

ANTONIA, R. A., BROWNE, L. W. B. & BISSET, D. K. 1987*b* *Proc. Sixth Symp. on Turbulent Shear Flows, Toulouse*, pp. 3.10.1–3.10.5.

ANTONIA, R. A., CHAMBERS, A. J., BRITZ, D. H. & BROWNE, L. W. B. 1986 *J. Fluid Mech.* **172**, 211–229.

ANTONIA, R. A., FULACHIER, L., KRISHNAMOORTHY, L. V., BENABID, T. & ANSELMET, F. 1988 *J. Fluid Mech.* **190**, 217–240.

ANTONIA, R. A., RAJAGOPALAN, S., SUBRAMANIAN, C. S. & CHAMBERS, A. J. 1982 *J. Fluid Mech.* **121**, 123–140.

BLACKWELDER, R. F. & KOVASZNAY, L. S. G. 1972 *Phys. Fluids* **15**, 1545–1554.

BOGARD, D. G. & TIEDERMAN, W. G. 1986 *J. Fluid Mech.* **162**, 389–413.

BROWN, G. L. & THOMAS, A. S. W. 1977 *Phys. Fluids* **20**, S243.

BROWNE, L. W. B., ANTONIA, R. A. & BISSET, D. K. 1986 *Phys. Fluids* **29**, 3612–3617.

CHEN, C-H. P. & BLACKWELDER, R. F. 1978 *J. Fluid Mech.* **89**, 1–31.

COLES, D. 1982 In *Surveys in Fluid Mechanics* (ed. R. Narasimha & S. M. Deshpande), pp. 17–33. Indian Academy of Sciences, Bangalore.

COLES, D. 1984 In *Turbulence and Chaotic Phenomena in Fluids* (ed. T. Tatsumi) pp. 397–402. North-Holland).

DEKEYSER, I., FULACHIER, L. & VEROLLET, E. 1977 *J. Méc.* **16**, 605–623.

DUMAS, R. 1962 Contribution à l'étude des spectres de turbulence. Thèse de Doctorat ès Sciences, Université de Provence, Marseille.

FALCO, R. E. 1977 *Phys. Fluids* **20**, S214.

FLEISCHMANN, S. T. & WALLACE, J. M. 1984 *AIAA J.* **22**, 766–769.

FULACHIER, L. 1972 Contribution à l'étude des analogies des champs dynamique et thermique dans une couche limite turbulent. Thèse Docteur ès Sciences, Université de Provence.

FULACHIER, L., VEROLLET, E. & DEKEYSER, I. 1977 *Intl J. Heat Mass Transfer* **20**, 731–739.

HEAD, M. R. & BANDYOPADHYAY, P. 1981 *J. Fluid Mech.* **107**, 297–338.

HUSSAIN, A. K. M. F. 1983 *Phys. Fluids* **26**, 2816–2850.

HUSSAIN, A. K. M. F. 1986 *J. Fluid Mech.* **173**, 303–356.

KLINE, S. J. 1978 In *Coherent Structure of Turbulent Boundary Layers* (ed. C. R. Smith & D. E. Abbot) AFOSR/Lehigh University.

KLINE, S. J. & FALCO, R. E. 1979 *Workshop on Coherent Structure in Turbulent Boundary Layers, Rep.* CSL-80-1, AFOSR/MSU. Michigan State University.

KLINE, S. J., REYNOLDS, W. C., SCHRAUB, F. A. & RUNSTADLER, P. W. 1967 *J. Fluid Mech.* **30**, 741–773.

PERRY, A. E. & CHONG, M. S. 1982 *J. Fluid Mech.* **119**, 173–217.

PERRY, A. E. & CHONG, M. S. 1987 *Ann. Rev. Fluid Mech.* **19**, 125–155.

RAJAGOPALAN, S. & ANTONIA, R. A. 1979 *Phys. Fluids* **22**, 614–622.

RAJAGOPALAN, S., SUBRAMANIAN, C. S., ANTONIA, R. A. & CHAMBERS, A. J. 1982 *Phys. Fluids* **25**, 1144–1145.

SUBRAMANIAN, C. S., RAJAGOPALAN, S., ANTONIA, R. A. & CHAMBERS, A. J. 1982 *J. Fluid Mech.* **123**, 335–362.

THOMAS, A. S. W. 1977*a* Organised structures in the turbulent boundary layer. PhD thesis, University of Adelaide.

THOMAS, A. S. W. 1977*b* In *AGARD CP*271, pp. 26–1–26–11.

THOMAS, A. S. W. & BROWN, G. L. 1977 *Proc. 6th Australasian Hydraulics & Fluid Mech. Conf.* Adelaide, pp. 407–410.

TOWNSEND, A. A. 1987 *PhysicoChemical Hydrodyn.* **5**, 23–30.

VEROLLET, E. 1972 Etude d'une couche limite turbulente avec aspiration et chauffage à la paroi. Thèse de Doctorat ès Sciences, Université de Provence, Marseille.

WILLMARTH, W. W. 1975 *Adv. Appl. Mech.* **15**, 159–254.